ICAS-88-3.10.4 TRANSONIC MAGNUS FORCE ON A FINNED CONFIGURATION

M. Ringel and A. Seginer
Faculty of Aeronautical Engineering
Technion - Israel Institute of Technology
Haifa 32000, Israel.

Abstract

Magnus forces are measured on a rotating Basic-Finner configuration at subsonic and transonic speeds. At low angles of attack no significant Magnus forces were observed in the subsonic regime, and "non-classic" Magnus forces were measured at transonic speeds. At higher angles of attack "non-classic" Magnus forces were measured at all Mach numbers. These were related to the side forces that existed on the non-rolling model under the same conditions.

Nomenclature

- b - span of the fins, 3d
- C_y - side (and Magnus) force coefficient, Y/qS
- d - model diameter
- f - spin frequency, RPS
- M - free-stream Mach number
- P - reduced spin rate, $2\pi fb/2V$
- q - free-stream dynamic pressure
- S - body cross-section area, $\pi d^2/4$
- V - free-stream velocity
- Y - side force (classic Magnus force here is Y>0)
- α - angle of attack
- δ_e - fin cant angle

I. Introduction

Typical fin-stabilized missile configurations are rotated around their longitudinal axes in order to average out geometrical and mass-distribution asymmetries or thrust misalignments. When the axis of rotation is inclined to the oncoming flow, this rotation can produce a side force and a yawing moment that are named after Magnus[1].

Because the Magnus phenomena affect the dynamic stability of the projectile[2], they were investigated experimentally quite extensively[1,3-5]. These investigations led to the formulation of four mechanisms that could cause the Magnus phenomena. Two of those mechanisms, that were concerned with the different base pressures and with the anti-symmetric axial components of the normal forces that acted on opposing fins, were believed to generate pure Magnus moments (pure couples) of a consistent sense[5]. Two other mechanisms were related to nonlinear interactions of the leeward fin with the viscous wake of the body and with the asymmetric vortex pair shed by it[1,4,6]. These latter mechanisms were believed to be responsible for an asymmetry in the side force on the leeward and windward fins and, therefore, also for a net Magnus force. Because of the nonlinear characters of these mechanisms, the Magnus force could reverse its sign under certain conditions[6].

Most of the experimental investigations were either on supersonic missile configurations or on low-subsonic bomb configurations. Very little data was available on finned missile configurations in the transonic flight regime, where most short-range air-to-air missiles operated. To fill this gap Seginer and Rosenwasser[6] investigated the Magnus phenomena on a "basic finner" configuration[3] at transonic speeds. Their main conclusion was that whereas the Magnus force and moment act in their classic direction in subsonic flow, all the configurations reversed the directions of the Magnus force and moment above some critical Mach number. This critical Mach number was dependent on the spin rate and on the angle of attack.

The final conclusion of Ref. 6 was that more data were required on the effects of the reduced spin rate on the Magnus phenomena. Consequently, a new model was built for the present investigation, that could be tested at many different fin cant angles. The results of the experiments with this model, that are presented in the present paper, raised more questions than answers.

II. Apparatus and Test Procedure

The experiments were conducted in the same 0.5m x 0.8m ventilated induction-type transonic wind tunnel, that also was used in Ref. 6. The model was the same Basic Finner configuration[3] also used there (Fig. 1), with the same outer diameter of d=45mm. However, whereas the model of Ref. 6 had integral fins (machined together with the body from the same steel rod in one piece), at two discrete cant angles only (δ_e= 3 and 7 degs), the fins of the new model were separate from the body and their cant angle could be varied continuously from zero to 40 degrees (Fig. 2).

The model was mounted on a standard six-component wind-tunnel balance via a

bearing-supported free-spinning sleeve. An optical revolution counter, built into the bearing house, measured the spin rate. This measuring system on rotating models was a much improved version of the one used in Ref. 6. Its design details and performance characteristics are described in Ref. 7.

The output from the balance and revolution counter, as well as from the tunnel-parameter transducers, was sampled at a rate of 10,000 Hz. The output from the revolution counter and from the balance was reduced to dimensionless coefficients. The spin frequency f, obtained by integration of the revolution-counter output, was reduced to its dimensionless form $P=2\pi fb/2V$. Forces and Moments were reduced to the conventional aerodynamic coefficients, using the free-stream dynamic pressure and the the body cross-section area and body diameter as normalizing area and length respectively. For the sign convention a right-hand body coordinate system was used. The x axis coincided with the model longitudinal axis, which was also its axis of rotation, and was positive pointing downstream. The z axis, normal to the x axis, was in the pitch plane and was positive pointing upward. The y axis was positive, pointing to starboard. With a positive spin, which in this coordinate system was anti-clockwise, facing upstream, the "classic" Magnus force would be positive or pointing to starboard. This means that the results to be presented here that have a positive side-force coefficnt, $C_y>0$, have the classic Magnus sense.

Before commencing a comprehensive parametric investigation with the new model it was decided to rerun the experiments of Ref. 6 and to compare the results. Consequently, the tests were conducted at the four Mach numbers, M=0.6, 0.85, 0.95 and 1.1, at which also the tests of Ref. 6 were run, with the fins at two cant angles δ_e= 3 and 7 degs[6]. Angle of attack sweeps were conducted with a locked model, in order to get the base-line data of the non-rotating model. The experiments with a rotating model were conducted in several modes. In some cases the model was locked during the tunnel start-up. When the Mach number stabilized, the lock on the model was released and the Magnus force (as well as all other forces and moments) was measured during the spin-up process at a fixed angle of attack. In other tests the results of pitch-and-pause measurements were compared with those of continuous angle-of-attack sweeps from α = - 4 deg to α = 12 deg. The conclusion of Ref. 6 that the model spin rate did not depend on the angle of attack but only on the Mach number and on the first differential angle, was confirmed. Consequently, most of the tests were angle-of-attack sweeps. Also confirmed was the conclusion of Ref. 16 that whereas the spin frequency, f, increased with the increasing Mach number, the reduced spin rate P remained approximately constant, and was dependent on the differential cant angle of the fins only.

III. Results and Discussion

Table I and Fig. 3 present the spin frequencies, f, and the reduced spin rates, P, for all four Mach numbers at both cant angles. Also presented, for comparison, are the results of Ref. 6. As expected the spin frequency increases both when the Mach number or the cant angle are increased. The reduced spin rate is, however, dependent on cant angle nly, and the variation with the Mach number seems to be within the scatter of the data.

The spin frequencies, and consequently also the reduced spin rates, that were measured in this work were lower than those reported by Ref. 6 for the same configuration. This difference must be the result of the difference in fin structure of both models. Whereas the fins of the model of Ref. 6 were integral, the fins of the present model have gaps between them and the body. Some loss of the pressure load on the fins (generally assumed to be about 10%), must therefore be expected, resulting in a lower rolling moment on the model and a lower steady-state spin rate.

The variations of the side-force coefficient, C_y, with the angle of attack and with the Mach number as an additional parameter, are presented in Figs. 4 and 5 for cant angles δ_e= 7 deg and 3 deg respectively. The curves, presented in these figures, are schematic only. Due to some as yet unidentified reason, there were fluctuations in the output that caused a considerable scatter in the data. The typical scatter in C_y was sometimes as large as ± 0.02. The curves were hand-faired through the average values of the data, to emphasize trends only, whereas the absolute values were in doubt. Furthermore, the raw output curves were all biased in the negative direction, i.e. for α=0 all output curves showed a non-zero, negative value for C_y. Because such a bias is unjustified, the curves were shifted to C_y=0 at α=0.

In search for the reasons for the bias and for the scatter in the data, it was decided to repeat some of the angle-of-attack sweeps, with the δ_e= 3 deg configuration, with the model prevented from rotating. The side-force coefficients obtained from these

experiments are presented Fig. 6. The results from the non-rotating model had a wide band of scatter (not shown here) similar to that of the the rotating-model results. The scatter was, therefore, not caused by the spinning motion (e.g. by an imbalanced model). The model also had a relatively large side-force coefficient in the negative direction at α=0, where no such force should exist. This large negative bias of -0.13 to -0.16 in the side-force coefficient, was reduced to about -0.03 by the rotation of the body, which averages out asymmetries in the models, but was not completely eliminated.

The parasitic side force on the non-rotating model (Fig. 6) had a positive gradient at low angles of attack, but at a certain value of α, a sharp break occurred in the curve and the side-force coefficient became increasingly more negative as the angle of attack increased. This latter part of the curve was apparently due to asymmetric vortex shedding that occurs on slender bodies at high incidence. It is interesting to note that the angle of attack of the break in C_y was decreasing when the Mach number was increased, and the slope of the curve after the break was decreasing too.

In comparing Figs. 5 and 6 one can see that the side-force-coefficient curves of the rotating model, break at approximately the same angles of attack as those of the non-rotating model. Similar breaks, although less pronounced, can be found in the results of the spinning model with δ_e= 7 deg (Fig. 4). The slopes of the curves after the break point for δ_e= 7 and 3 deg are similar. One must conclude that all side-force results at angles of attack that are higher than those of the respective break points, are mainly caused by the asymmetric vortices of the non-rotating body.

At angles of attack below the break point, the side-force coefficients at the Mach numbers M = 0.6, 0.8 are sufficiently small, compared with the data scatter, to be considered insignificant (Figs. 4,5). This is in contrast with Ref. 6 where the side forces had the classic Magnus sense in this Mach number range at δ_e = 7 deg. The side-force coefficient values are significant at M = 1.1 and somewhat less significant at M = 0.95. In both these cases, for both δ_e = 7 and 3 deg, the slope of C_y vs. α is negative, which means that the side force acts in the direction that is opposite to the classic Magnus force. This is in agreement with the conclusions of Ref. 6.

In making the above comparisons with Ref. 6, one has to remember the difference between the two models in the fin construction.

The apparent negligible side forces at the subsonic Mach numbers, where Ref. 6 stated to have measured Magnus forces acting in the classic direction, raise again the question why such forces should act on the fins in the first place. Asymmetries in the flow on the anti-symmetric deflected fins could generate Magnus effects. Such asymmetries in the effective flow over the fins occur only while the spin rate is building up. Steady spin rate is reached when the rolling moment vanishes. This happens when the effective angles of attack on both fins are identical (assuming zero friction in the bearings). Under these conditions the flow over the fins is symmetrical, and no Magnus phenomena should exist, as long as the angle of attack is small and there are no non-linear interactions of the leeward vertical fin with the viscous or vortical wake. On the other hand, with significant friction in the bearings, a steady spin rate will be reached when the aerodynamic forcing rolling moment is finite and equal (and opposite) to the frictional damping moment. When this happens, the effective angles of attack on the fins are not equal, and the resulting flow asymmetries could generate Magnus effects. This means that Magnus data from identical finned models, on different spin systems, may differ because of unequal friction in the bearings of the different systems.

This hypothesis could explain the difference between the present subsonic results with a new and improved Magnus system, and those of Ref. 6 that were obtained with the older system. Figure 7 is presented to validate this hypothesis. It shows the time-history of the side-force coefficient of the present model with δ_e= 12 deg at M=0.6 and α=0. The model reached a steady reduced spin rate of about P = 0.29 in one second and later maintained a constant spin rate and side-force (this constant value of $C_y \cong -0.06$ is apparently the bias). During the acceleration phase the side force coefficient is seen to first increase, and then gradually vanish as steady-state symmetrical conditions are reached.

IV. Conclusions

Doubts have been raised as to the existence of Magnus phenomena on the spinning basic finner configuration at subsonic speeds and low angles of attack, that are characteristic of the fins and not of the slender body. At transonic speeds (M = 0.95, 1.1) a Magnus force existed and was opposed to the classic sense. At higher angles of attack

"non-classic" Magnus forces were observed at all test Mach numbers. These were apparently related to the asymmetric vortex wake of the slender body.

More carefully acquired data are needed for a better understanding of the various phenomena.

V. References

1. Platou, A.S., "Magnus Characteristics of Finned and Nonfinned Projectiles", AIAA Journal, Vol. 3, Jan. 1965, pp. 83-90.

2. Murphy, C.H., "Effect of Roll on Dynamic Instability of Symmetric Missiles", Journal of the Aeronautical Sciences, Vol. 21, Sept. 1959, pp. 643-644.

3. Nicolaides, J.D., Eikenberry, R.S., Ingram, C.W., and Clare, T.A., "Flight Dynamics of the Basic Finner Missile", AFATL, Eglin Air Force Base, Fla., Report No. TR-68-82, July 1968.

4. Uselton, J.C. and Carman, J.B., "A Study of the Magnus Effects on a Sounding Rocket at Supersonic Speeds", Journal of Spacecraft and Rockets, Vol. 8, Jan. 1971, pp. 28-34.

5. Benton, E.R., "Supersonic Magnus Effect on a Finned Missile", AIAA Journal, Vol. 2, Jan. 1964, pp. 153-155.

6. Seginer, A. and Rosenwasser, I., "Magnus Effects on Spinning Transonic Finned Missiles", Journal of Spacecraft and Rockets, Vol. 23, Jan.-Feb. 1986, pp. 31-38.

7. Ringel, M., Levin, D., and Seginer, A., "A Modified Experimental System for Measurement of Magnus Loads", Experiments in Fluids, Vol. 3, July 1985, pp. 209-214.

8. Levin, D. and Seginer, A., "Wing-Body Interaction for Small Span Delta Wings", Israel Journal of Technology, Vol. 13, May 1975, Nos. 1-2.

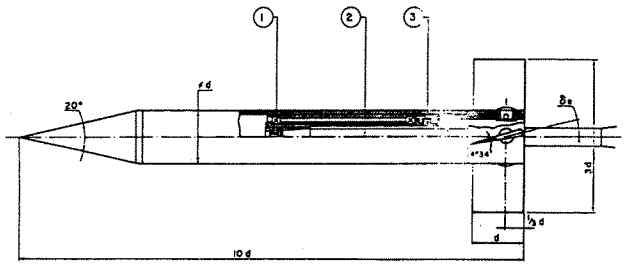

Fig. 1. The basic finner with canted fins.

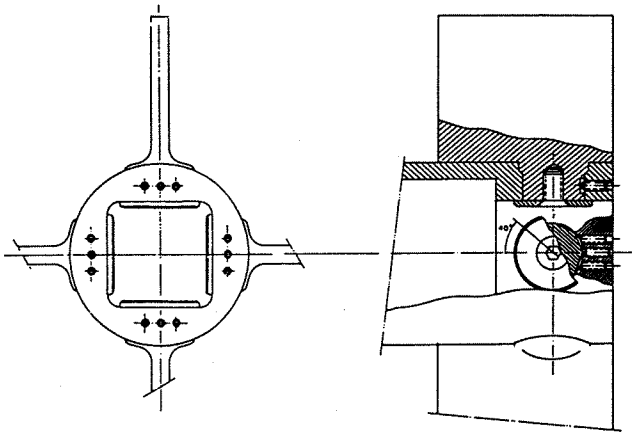

Fig. 2. The present model with variable cant angle.

M	PRESENT RESULTS				REF. 6			
	δ_e= 3 deg		δ_e= 7 deg		δ_e= 3 deg		δ_e= 7 deg	
	f	P	f	P	f	P	f	P
0.60	29	0.060	74	0.154	37	0.077	85	0.176
0.85	42	0.062	90	0.132	48	0.070	112	0.165
0.95	50	0.065	112	0.147	55	0.072	130	0.170
1.10	53	0.061	120	0.137	65	0.075	150	0.170

TABLE 1 - SPIN FREQUENCIES AND REDUCED SPIN RATES

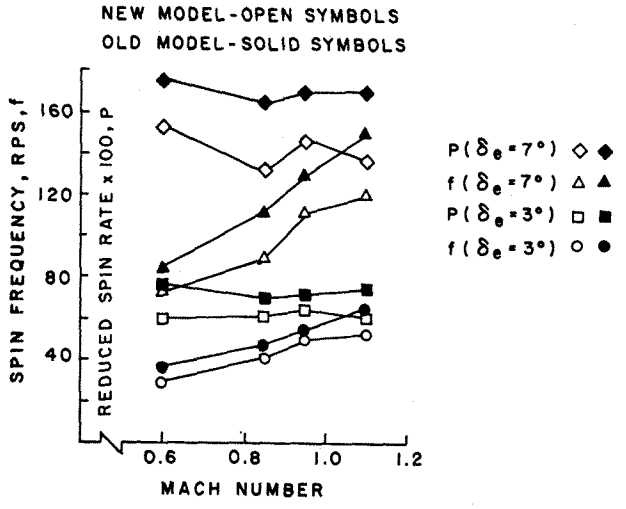

Fig. 3. Spin frequencies and reduced spin rates.

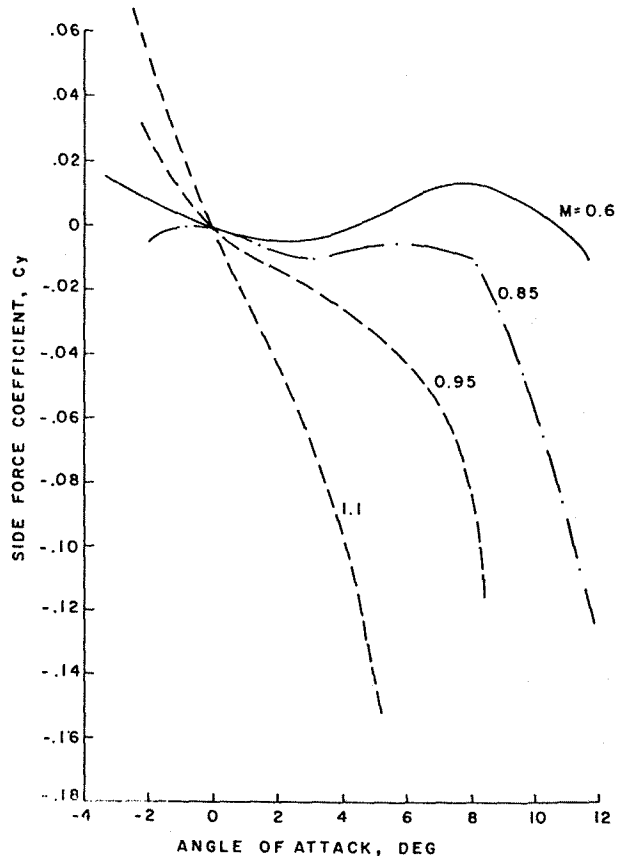

Fig. 4. Side-force coefficient at $\delta_e=7^\circ$.

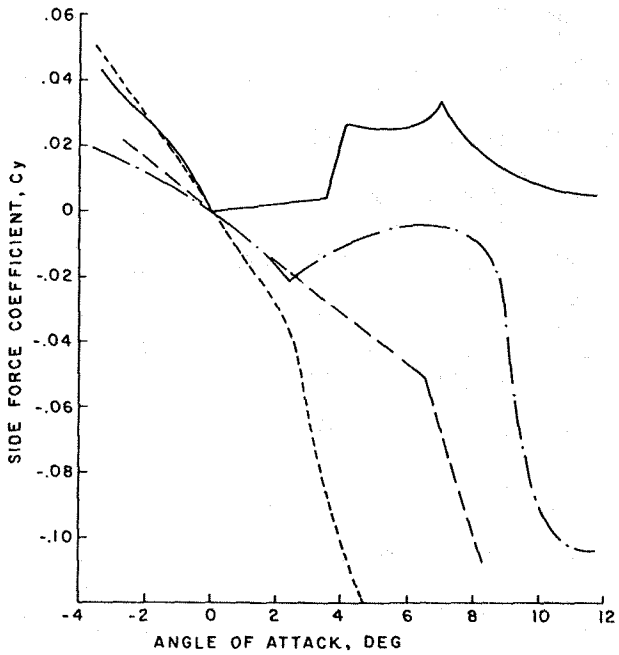

Fig. 5. Side-force coefficient at $\delta_e=3^\circ$.

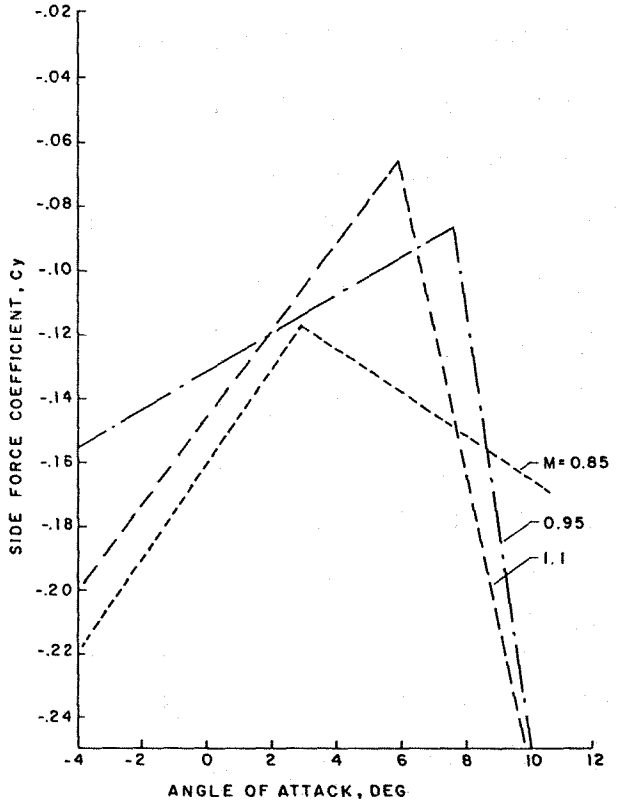

Fig. 6. Side-force coefficient, model not rotating.

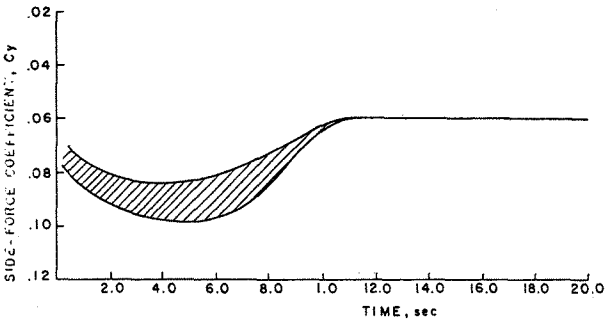

Fig. 7. Time-history of the side-force coefficient, M=0.6, α=0, δ_e=12 deg.